Minimum-Current-Stress Scheme of Dual Active Bridge DC–DC Converter With Unified Phase-Shift Control

Nie Hou, Wensheng Song, *Member, IEEE*, and Mingyi Wu

***Abstract*—To reduce current stress and improve efficiency of dual active bridge (DAB) dc–dc converters, various control schemes have been proposed in recent decades. Most control schemes for directly minimizing power losses from power loss modeling analysis and optimization aspect of the adopted converter are too difficult and complicated to implement in real-time digital microcontrollers. Thus, this paper focuses on a simple solution to reduce current stress and improve the efficiency of the adopted DAB converter. However, traditional current-stress-optimized (CSO) schemes have some drawbacks, such as inductance dependency and an additional load-current sensor. In this paper, a simple CSO scheme with a unified phase-shift (UPS) control, which can be equivalent to the existing conventional phase-shift controls, is proposed for DAB dc–dc converters to realize current stress optimization. The simple CSO scheme can overcome those drawbacks of traditional CSO schemes, gain the minimum current stress, and improve efficiency. Then, a comparison of single-phase-shift (SPS) control, simple CSO scheme with dual-phase-shift (CSO-DPS) control, simple CSO scheme with extended-phase-shift (CSO-EPS) control, and simple CSO scheme with UPS (CSO-UPS) control is analyzed in detail. Finally, experimental results verify the excellent performance of the proposed CSO-UPS control scheme and the correctness of theoretical analysis.**

***Index Terms*—Current sensorless, current stress, inductance independency, optimization, unified phase-shift control.**

I. Introduction

At the beginning of the 1990s, the dual active bridge (DAB) dc–dc converter was originally proposed in [1], as shown in Fig. 1. Due to these advantages of high power density, zero-voltage switching (ZVS), bidirectional power flow capability, and the convenience of cascaded or paralleled modularity, DAB dc–dc converters have attracted more and more attention in power energy conversion application, such as distributed generating systems, hybrid systems, and dc microgrid [2]–[15].

Phase-shift control has become the most popular scheme for DAB dc–dc converters. According to the number of phase-shift angles, traditional phase-shift-control can be mainly classified as single-phase-shift (SPS) and dual-phase-shift (DPS). SPS control, due to being easy to implement, has been widely applied in DAB dc–dc converters [15], [16]. However, the performance of DAB dc-dc converter is a little bit poor by using SPS control, especially when the input and output voltage amplitudes of the isolated transformer are serious unequal [17]. In this case, the current stress becomes much high, which results in an increase of device cost such as the need for a large magnetic core in high input voltage and light-load conditions, and the excessive current stress may bring low efficiency and even the damage of power devices in DAB dc–dc converters [18].

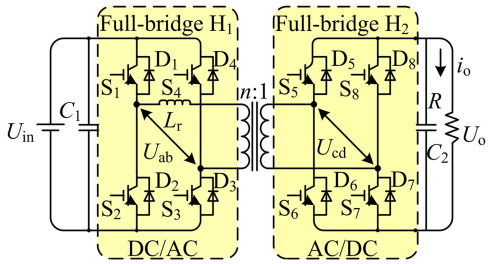

Fig. 1. Topology of a DAB dc–dc converter

In order to overcome these drawbacks of SPS control, a DPS control scheme [18] is proposed to eliminate reactive power, reduce current stress, and improve efficiency. But phase-shift ratios reported in [18] are not optimized. Moreover, transmission power characterization and dynamic performance of the DPS control are discussed in [19] and [20]. The DPS control scheme with optimization compensation, which is applied in DAB dc–dc converters, is proposed to reduce reactive power and current stress [21]. On the basis of this, an extended-phase-shift control is proposed to reduce current stress and reactive power of DAB dc–dc converters [22]. Then, a current-stress-optimized (CSO) switching strategy of DAB dc–dc converters with DPS control is proposed in [23], where the CSO scheme is discussed to reduce current stress and increase efficiency.

Some methods that allow DAB dc–dc converters to operate with soft-switching in the full operating range are proposed to reduce switching losses and improve efficiency significantly [24], [25]. In addition, power loss analysis and efficiency optimization strategy are reported in [11], [26], and [27], where the power loss modeling of DAB dc–dc converters is adopted to predict the dissipated power. On this basis, an efficiency-optimized switching strategy is proposed. However, the realization processes of efficiency-optimized switching strategies [11], [26], [27] are inconvenient and complicated in real-time

Manuscript received July 13, 2015; revised October 03, 2015 and December 02, 2015; accepted January 11, 2016. Date of publication January 25, 2016; date of current version July 08, 2016. This work was supported in part by the National Natural Science Foundation of China under Project 51577160. Recommended for publication by Associate Editor Dmitri Vinnikov. *(Corresponding author: Wensheng Song.)*

The authors are with the School of Electrical Engineering, Southwest Jiaotong University, Chengdu 610031, China (e-mail: nie_hou@126.com; songwsh@swjtu.edu.cn; 1536689170@qq.com).

Color versions of one or more of the figures in this paper are available online at http://ieeexplore.ieee.org.

Digital Object Identifier 10.1109/TPEL.2016.2521410

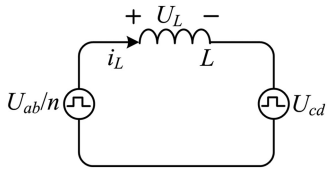

Fig. 2. Equivalent topology of DAB dc–dc converters with the phase-shift control

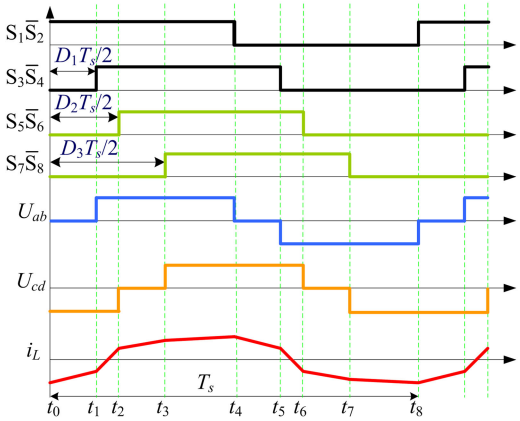

Fig. 3. Waveforms of DAB dc–dc converters with UPS control

digital microprocessors. Thus, in order to simplify power loss model, literatures [28], [29] propose a phase-shift solution by reducing the root-mean-square (rms) value of the inductor current. In order to reduce the rms value of the inductor current, the phase-shift ratios in [29] should be calculated off-line by mathematical software, due to its complexity. In addition, the dominant conduction loss is conducting loss of power devices IGBTs, and not copper loss of the auxiliary inductors and the high-frequency transformer [30]. The dominant conduction loss is related to the average value of inductor current with absolute value dispose [26], [27], [30].

Moreover, optimizing current stress and reactive power simultaneously, the proposed control scheme in [21] fails to reduce current stress, effectively. Although the CSO scheme with EPS (CSO-EPS) control in [22] can significantly reduce the current stress, it is too difficult to implement by using the traditional CSO scheme [31]. Because the phase-shift ratios in CSO-EPS control are not monotonically increased or decreased with control variables, and these phase-shift ratios are required to be off-line estimated. In addition, there are some drawbacks such as the inductance dependency and an additional load-current sensor in the adopted CSO-DPS scheme to estimate transmission power [23].

On the basis of the aforementioned analysis, focusing on current stress reduction, a simple CSO scheme is proposed to overcome these drawbacks of traditional CSO scheme in this paper. And the simple CSO scheme with a unified phase-shift (CSO-UPS) control is discussed in detail. Moreover, the UPS control can be equivalent to other common phase-shift controls, such as SPS [1], DPS [18], and EPS [22] control schemes. And a comparison of SPS control, the simple CSO-DPS control,

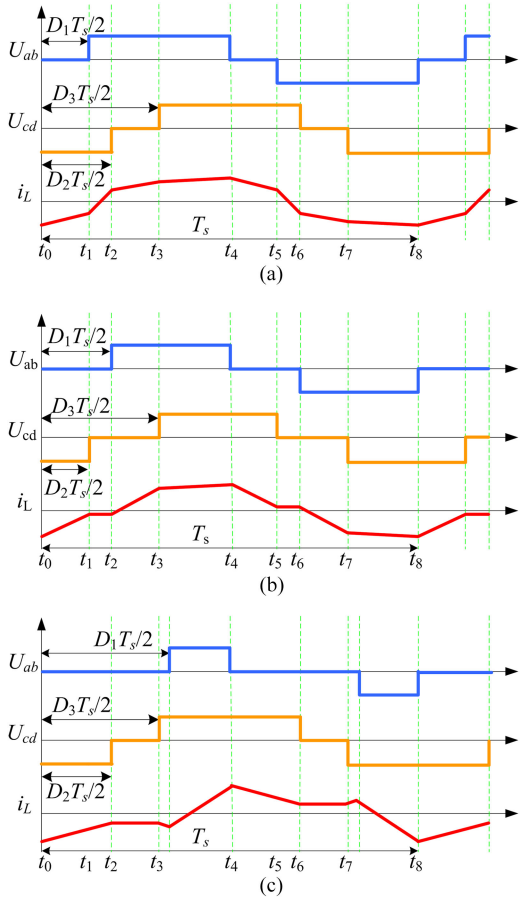

Fig. 4. Waveforms of DAB dc–dc converters with UPS control. (a) $0 \le D_1 \le D_2 \le D_3 \le 1$. (b) $0 \le D_2 \le D_1 \le D_3 \le 1$. (c) $0 \le D_2 \le D_3 \le D_1 \le 1$.

the simple CSO-EPS control, and the simple CSO-UPS control schemes is discussed in detail.

The paper is organized as follows. In Section I, an introduction is given. In Section II, the UPS control is analyzed in detail. The simple CSO scheme is proposed and discussed in Section III, and on the basis of UPS control, the relationship of SPS control, simple CSO-DPS control, simple CSO-EPS control and simple CSO-UPS control is discussed. A comparison of current stress in these four controls is analyzed, and an efficiency analysis and comparison among these four schemes are shown in Section IV. In Section V, experimental results of these control schemes are shown and compared to verify the effectiveness of theoretical analysis.

II. Switching-Mode Analysis of UPS Control

The equivalent topology of DAB dc–dc converters with the phase-shift control is shown in Fig. 2, where L is the total value of the transformer leakage inductor and auxiliary inductor L_r, $U_{\rm ab}$, and $U_{\rm cd}$ represent the output pulse voltage of $H1$ bridge and the input pulse voltage of $H2$ bridge, respectively; U_L and i_L, respectively, represent the voltage and current of inductor L.

The main curves of switching sequences, current, and voltages in DAB dc–dc converters with UPS control are shown

TABLE I
VALUE OF U_L IN A HALF OF SWITCHING CYCLE

$0\le D_1\le D_2\le D_3\le 1$		$0\le D_2\le D_1\le D_3\le 1$		$0\le D_2\le D_3\le D_1\le 1$	
Time interval	U_L	Time interval	U_L	Time interval	U_L
0-$D_1T_s/2$	nU_o	0-$D_2T_s/2$	nU_o	0-$D_2T_s/2$	nU_o
$D_1T_s/2$-$D_2T_s/2$	$U_{in}+nU_o$	$D_2T_s/2$-$D_1T_s/2$	0	$D_2T_s/2$-$D_3T_s/2$	0
$D_2T_s/2$-$D_3T_s/2$	U_{in}	$D_1T_s/2$-$D_3T_s/2$	U_{in}	$D_3T_s/2$-$D_1T_s/2$	$-nU_o$
$D_3T_s/2$-$T_s/2$	U_{in}-nU_o	$D_3T_s/2$-$T_s/2$	U_{in}-nU_o	$D_1T_s/2$-$T_s/2$	U_{in}-nU_o

in Fig. 3, where T_s represents a switching cycle, D_1 represents the phase-shift ratio between S_1 and S_3, D_2 represents the phase-shift ratio between S_1 and S_5, and D_3 represents the phase-shift ratio between S_1 and S_7. Phase-shift ratios are all referred to the same reference modulation signal S_1, which is different from the existing phase-shift controls and convenient to be implemented in digital control by using DSP or FPGA chips.

Even if D_2 is larger or smaller than D_3, the same values of voltage $U_{\rm cd}$ and current i_L can be obtained, and the transmission powers are identical. Thus, D_2 can be configured less than D_3 to simplify phase-shift ratio conditions, and the waveforms of DAB dc–dc converters with UPS control can be shown in Fig. 4.

Applying Kirchhoff voltage law (KVL) in circuit topology shown in Fig. 2, the expressions of i_L can be expressed as

$$\frac{di_L(t)}{dt}=\frac{U_L(t)}{L}=\frac{U_{\rm ab}(t)-U_{\rm cd}(t)}{L}. \tag{1}$$

From Fig. 4, the average transmission power of DAB dc–dc converter with UPS control can be expressed as

$$P=\frac{1}{T_s}\int_0^{T_s}U_{\rm ab}(t)i_L(t)dt. \tag{2}$$

Assuming that $t_0=0$ at the beginning of the switching cycle in Fig. 4, the inductance voltage U_L in each time interval is shown in Table I.

Assuming that $k=U_{\rm in}/nU_o$ and $k\ge 1$ in this paper, the other condition $k<1$ can be analyzed similarly. Then, considering the average inductor current during each switching cycle T_s should be zero in steady state, combining (1) and Table I, for the convenience of analysis, the current stress during a half of switching cycle is equivalent to $i_L(t_4)$ and can be derived and unified as

$$i_p=\frac{i_P}{i_N}=2[D_2+D_3-1+k(1-D_1)] \tag{3}$$

where i_N is defined as

$$i_N=\frac{T_sU_o}{8L}. \tag{4}$$

From (2) and Table I, for the convenience of analysis, the transmission power P of the DAB dc–dc converter with UPS control can be expressed and unified as

$$p=\frac{P}{P_N}=\begin{cases}2(-D_1+D_2+D-D_1^2\\ -D_2^2-D_3^2+D_1D_2+D_1D_3) & (D_1\le D_2\le D_3\le 1)\\ 2(-D_1+D_2+D_3\\ +D_1D_3-D_3^2-D_1D_2) & (D_2\le D_1\le D_3\le 1)\\ 2(-D_1+D_2+D_3\\ +D_1^2-D_1D_2-D_1D_3) & (D_2\le D_3\le D_1\le 1)\end{cases} \tag{5}$$

where P_N is defined as

$$P_N=\frac{nT_SU_{\rm in}U_o}{8L}. \tag{6}$$

In Fig. 4, if $D_1=D_3-D_2$, the UPS control is equivalent to the DPS control [15]. If $D_1=0$ and $D_3=D_2$, the UPS control is equivalent to the SPS control [1]. If $D_1=0$ or $D_3=D_2$, the UPS control is equivalent to the EPS control [22]. Moreover, almost all of these current stress reduction schemes [17], [18], [22], [23] are be realized by using the cases $0\le D_1\le D_2\le D_3\le 1$ and $0\le D_2\le D_1\le D_3\le 1$ of the UPS control. And the case $0\le D_2\le D_3<D_1\le 1$ can guarantee adequate current for ZVS and may be suitable to realize the soft switching [25]. Thus, this paper focuses on the cases $0\le D_1\le D_2\le D_3\le 1$ and $0\le D_2\le D_1\le D_3\le 1$ to reduce the current stress of the adopted converter.

III. PROPOSED SIMPLE CURRENT-STRESS-OPTIMIZED SCHEME

Limited to the traditional control theory, in the traditional CSO schemes, one of the phase-shift ratios (such as D_2) should be monotonically increased along with the transmission power, which can ensure a linear controller (such as PI) is available to regulate the output voltage or transmission power [23], [31]. And the others phase-shift ratios should be calculated with accurate system parameters requirement, such as inductance, as shown in Fig. 5. Unfortunately, the inductance parameter mismatch will have an effect on the control performance of CSO

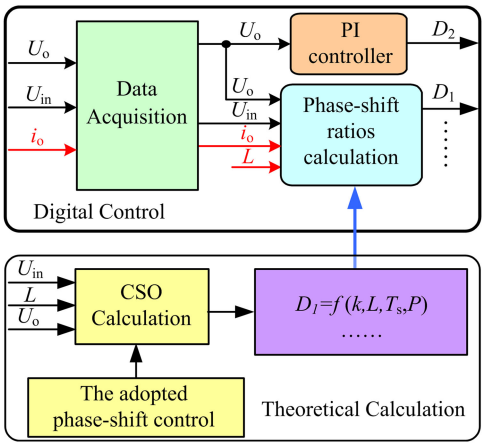

Fig. 5. Block diagram of traditional CSO scheme for DAB converters.

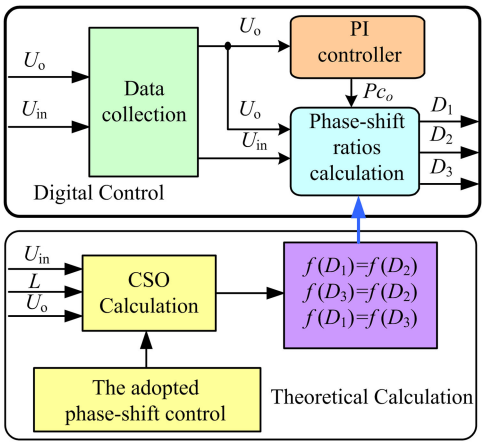

Fig. 6. Block diagram of the proposed simple CSO scheme for DAB converters.

scheme. In addition, none of phase-shift ratios is monotonically increased along with the transmission power. Thus, the traditional CSO control scheme is complicated and requires the off-line calculation [22].

In order to overcome drawbacks of traditional CSO scheme, a simple CSO scheme is proposed, as shown in Fig. 6, where Pc_o represents the output value of PI voltage controller. The keynote of the simple CSO scheme is that the optimal control can be achieved through utilizing the specific relationship of the phase-shift ratios in different phase-shift controls, and the current stress is expressed by phase-shift ratios without higher order terms. Thus, the simple relationship of phase-shift ratios D_1–D_3 can be obtained by using Lagrange multiplier method (LMM), which is one of the popular optimization methods to solve extreme value condition.

From Fig. 6, in order to reduce current stress of DAB dc–dc converters, the relationship among D_1, D_2, and D_3 should be described first by using LMM in the simple CSO control and described as

$$E = i_p + \lambda(p - p^*) \tag{7}$$

where E is the Lagrangian function, λ is the Lagrangian multiplier, and p^* is the desired and unified transmission power. According to (5), (6), and (7), the relationship among D_1, D_2, and D_3 can be obtained from (8) by LMM

$$\begin{cases} \dfrac{\partial E}{\partial D_1} = 0 \\ \dfrac{\partial E}{\partial D_2} = 0 \\ \dfrac{\partial E}{\partial D_3} = 0. \end{cases} \tag{8}$$

In UPS control (the cases $0 \le D_1 < D_2 \le D_3 \le 1$ and $0 \le D_2 \le D_1 \le D_3 \le 1$), D_2 and D_3 can be deduced from (8) with an expression of D_1 as (9). Actually, the case $0 \le D_2 \le D_3 \le D_1 \le 1$ is unsolvable from (8)

$$\begin{cases} D_2 = \begin{cases} (k-1)(1-D_1) & \left(0 \le p < 2\dfrac{k-1}{k^2}\right) \\ \dfrac{k-2}{2(k-1)}D_1 + \dfrac{1}{2} & \left(2\dfrac{k-1}{k^2} \le p \le 1\right) \end{cases} \\ D_3 = \begin{cases} D_1 & \left(0 \le p < 2\dfrac{k-1}{k^2}\right) \\ \dfrac{k-2}{2(k-1)}D_1 + \dfrac{1}{2} & \left(2\dfrac{k-1}{k^2} \le p \le 1\right). \end{cases} \end{cases} \tag{9}$$

In addition, when $D_1 = D_3 - D_2$, the UPS control is simplified as the DPS control. Similarly, D_2 and D_3 in DPS control can be expressed by D_1 as

$$\begin{cases} D_2 = \begin{cases} \dfrac{(k-1)(1-D_1)}{k+1} & \left(0 \le p < \dfrac{k^2+2k-3}{2k^2}\right) \\ -\dfrac{1}{k-1}D_1 + \dfrac{1}{2} & \left(\dfrac{k^2+2k-3}{2k^2} \le p \le 1\right) \end{cases} \\ D_3 = \begin{cases} \dfrac{2D_1+k-1}{k+1} & \left(0 \le p < \dfrac{k^2+2k-3}{2k^2}\right) \\ \dfrac{k-2}{k-1}D_1 + \dfrac{1}{2} & \left(\dfrac{k^2+2k-3}{2k^2} \le p \le 1\right) \end{cases} \end{cases}. \tag{10}$$

When $D_1 = 0$ and $D_2 = D_3$, the UPS control is simplified as the SPS control. Especially, when $k = 1$, both the UPS control and the DPS control can be equivalent to SPS control.

More importantly, the relationship between Pc_o and phase-shift ratios $D_1 - D_3$ should be discussed, and Pc_o is unified and ranged from 0 to 1 in this paper. In the adopted CSO-UPS control, according to (5) and (9), the phase-shift ratio D_1 can be expressed with respect to p as

$$D_1 = \begin{cases} 1 - \dfrac{\sqrt{2p(k-1)}}{2k-2} & \left(0 \le p < 2\dfrac{k-1}{k^2}\right) \\ \dfrac{(k-1)\sqrt{(1-p)(k^2-2k+2)}}{k^2-2k+2} & \left(2\dfrac{k-1}{k^2} \le p \le 1\right). \end{cases} \tag{11}$$

According to (11), D_1 is monotonically decreasing along with p. Combining (9) and (11), if $k > 2$, D_2 is first increased and then decreased along with p; and if $k < 2$, D_3 is first decreased

and then increased along with p. Only D_1 is monotonically varied along with p. Thus, D_1 can be equivalent to $(1 - Pc_o)$ to easily realize the CSO-UPS control by using PI controller, and Pc_o is monotonically increasing along with p. Then, (9) can be rewritten as

$$\begin{cases} D_1 = 1 - Pc_o & (0 \le Pc_o < 1) \\ D_2 = \begin{cases} (k-1)Pc_o & \left(0 \le Pc_o < \dfrac{1}{k}\right) \\ \dfrac{(2-k)Pc_o}{2(k-1)} + \dfrac{2k-3}{2(k-1)} & \left(\dfrac{1}{k} \le Pc_o \le 1\right) \end{cases} \\ D_3 = \begin{cases} 1 - Pc_o & \left(0 \le Pc_o < \dfrac{1}{k}\right) \\ \dfrac{(2-k)Pc_o}{2(k-1)} + \dfrac{2k-3}{2(k-1)} & \left(\dfrac{1}{k} \le Pc_o \le 1\right). \end{cases} \end{cases} \tag{12}$$

Similarly, in the simple CSO-DPS control, both of D_1 and D_2 are monotonically varied along with p, but D_2 is monotonically increased along with p. Thus, D_2 can be equivalent to $Pc_o/2$ to realize the CSO-DPS control, and (10) can be rewritten as

$$\begin{cases} D_1 = \begin{cases} -\dfrac{k+1}{2(k-1)}Pc_o + 1 & \left(0 \le Pc_o < \dfrac{1}{k}\right) \\ \dfrac{-(k-1)Pc_o}{2} + \dfrac{(k-1)}{2} & \left(\dfrac{1}{k} \le Pc_o \le 1\right) \end{cases} \\ D_2 = \dfrac{Pc_o}{2} & (0 \le Pc_o < 1) \\ D_3 = \begin{cases} -\dfrac{1}{k-1}Pc_o + 1 & \left((0 \le Pc_o < \dfrac{1}{k})\right) \\ \dfrac{-(k-2)Pc_o}{2} + \dfrac{(k-1)}{2} & \left(\dfrac{1}{k} \le Pc_o \le 1\right). \end{cases} \end{cases} \tag{13}$$

In SPS control, the phase-shift ratios D_1–D_3 can be expressed as

$$\begin{cases} D_1 = 0 \\ D_2 = \dfrac{Pc_o}{2} & (0 \le Pc_o < 1) \\ D_3 = \dfrac{Pc_o}{2}. \end{cases} \tag{14}$$

Moreover, a CSO-EPS control is proposed in [22], which can achieve a low current stress. Unfortunately, because the phase-shift ratios are not monotonically decreased or increased along with p, the computation and realization of the proposed CSO-EPS in [22] is a little bit complicated. Thus, like the implementation of the optimal control in [27], the phase-shift ratios must be calculated off-line by mathematical software first and then the calculated results are stored in a lookup table form of memory space in a microcontroller. The control scheme can search the optimum phase-shift ratios stored in table, on the basis of the detected output voltage, output current, and input voltage. In order to implement the CSO scheme, some prerequisite conditions in [22] should be satisfied and shown as

$$\begin{cases} \left(0 \le D < \dfrac{2-\sqrt{2}}{4}\right) \\ \quad \begin{cases} D_1' = \begin{cases} \dfrac{1-\sqrt{2(1-2D)^2-1}}{2} & k < 2 \\ \dfrac{1+\sqrt{2(1-2D)^2-1}}{2} & k \ge 2 \end{cases} \\ D_2' = 0 \end{cases} \\ \left(\dfrac{2-\sqrt{2}}{4} \le D < \dfrac{1}{2}\right) \begin{cases} D_1' = \dfrac{\sqrt{2}(1-2D)}{2} \\ D_2' = \dfrac{1-\sqrt{2}(1-2D)}{2} \end{cases} \end{cases} \tag{15}$$

where D_1' and D_2' are the phase-shift ratios in EPS control [22]. Then, according to (15), on the basis of UPS control concept, phase-shift ratios can be further expressed by using the simple CSO scheme as

$$\begin{cases} D_1 = \begin{cases} Pc_o & \left(k < 2, 0 \le Pc_o < \dfrac{1}{2}\right) \\ 1 - Pc_o & \begin{cases} (k \ge 2, 0 \le Pc_o < \dfrac{1}{2}) \\ \left(\dfrac{1}{2} \le Pc_o < 1\right) \end{cases} \end{cases} \\ D_2 = D_3 = \begin{cases} Pc_o & \left(k < 2, 0 \le Pc_o < \dfrac{1}{2}\right) \\ 1 - Pc_o & \left(k \ge 2, 0 \le Pc_o < \dfrac{1}{2}\right) \\ \dfrac{1}{2} & \left(\dfrac{1}{2} \le Pc_o < 1\right) \end{cases} \end{cases} \tag{16}$$

where $D_1 = D_1'$ and $D_2 = D_3 = D_1' + D_2'$. According to (16), the CSO-EPS can be implemented easily, and the amount of computation can be significantly decreased.

According to the aforementioned analysis, Fig. 7 shows the block diagram of DAB dc–dc converters with phase-shift controls to implement the CSO scheme, where U_o^* represents the desired output voltage. Because the CSO scheme is to improve performance of the DAB dc–dc converters at steady state, U_o^* is adopted to replace U_o in voltage ratio k calculation block to easily avoid that k is close to infinitely great, due to the very small value U_o at the start-up stage. And, it can ensure $k \ge 1$. Compared with the traditional CSO scheme, the adopted controller only requires the input voltage U_{in} and output voltage U_o as the feedback quantities in the adopted simple CSO scheme, which does not need an additional load-current sensor and inductance value L. It means that the adopted CSO scheme is not sensitive to inductor parameter L. Compared with the traditional CSO methods, the control model of the proposed simple CSO scheme is significantly simplified.

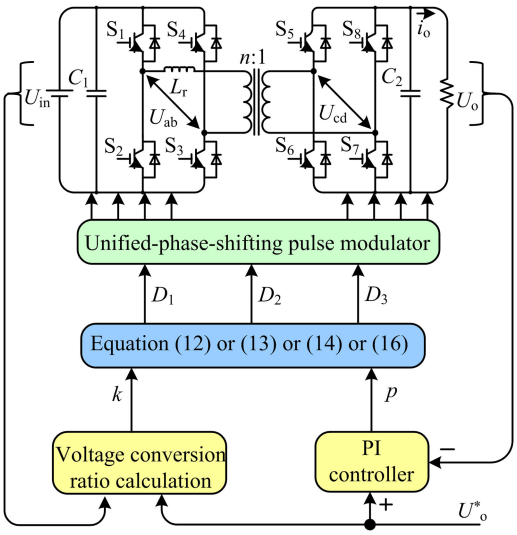

Fig. 7. Control system structure of DAB dc–dc converters with simple CSO scheme.

TABLE II
CURRENT STRESS OF SPS, CSO-DPS, CSO-EPS, AND CSO-UPS CONTROLS

Phase-shift controls	Range of p	Current stress i_p
SPS	$0 \le p \le 1$	$2(k-\sqrt{1-p})$
CSO-DPS	$0 \le p < \frac{k^2+2k-3}{2k^2}$	$\sqrt{(k-1)(6+2k)p}$
	$\frac{k^2+2k-3}{2k^2} < p \le 1$	$2k-\sqrt{(2k^2-4k+6)(1-p)}$
CSO-EPS	$0 \le p \le \frac{1}{2}$	$k+(2-k)\sqrt{1-2p}$
	$\frac{1}{2} < p \le 1$	$2k-k\sqrt{2-2p}$
CSO-UPS	$0 \le p \le 2\frac{k-1}{k^2}$	$2\sqrt{2p(k-1)}$
	$2\frac{k-1}{k^2} < p \le 1$	$2k-2\sqrt{(k^2-2k+2)(1-p)}$

IV. COMPARATIVE ANALYSIS AMONG SPS, CSO-DPS, CSO-EPS, AND CSO-UPS CONTROLS

A. Comparative Analysis of Current Stress

This section shows a comparative analysis of current stress among SPS, CSO-DPS, CSO-EPS, and CSO-UPS controls. The basic prerequisite for comparative analysis of the current stress is that the unified transmission power p, the input voltage U_{in}, and the output voltage U_o of SPS, CSO-DPS, CSO-EPS, and CSO-UPS controls are set to the same.

According to (3), (5), (9), (10), (15), and (16) and the phase-shift ratios $D_1 = 0$, $D_2 = D_3$ in SPS control, the current stress i_p in various control methods is shown in Table II.

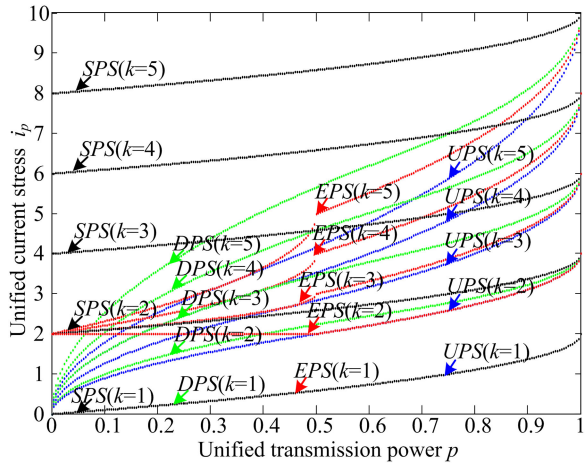

Fig. 8. Curves of unified current stress i_p with respect to p and k in SPS, CSO-DPS, CSO-EPS, and CSO-UPS controls.

According to Table II, the relation curves of the unified current stress i_p with respect to the unified transmission power p and the voltage conversion ratio k are shown in Fig. 8.

Fig. 8 shows that the relation curves of the unified current stress i_p with the unified transmission power p and voltage conversion ratio k in SPS, CSO-DPS, CSO-EPS, and CSO-UPS controls, respectively. As can be seen from Fig. 7, if the power p is invariable, the unified current stress i_p of SPS, CSO-DPS, CSO-EPS, and CSO-UPS controls increase with k. And if the ratio k is invariable, the unified current stresses i_p of SPS, CSO-DPS, CSO-EPS, and CSO-UPS controls increase with p, too. According to Fig. 8, the CSO-DPS, CSO-EPS, and CSO-UPS controls can generate smaller current stress i_p than the SPS control. More importantly, because the phase-shift ratio range of DPS and EPS controls are too confined to realize global optimization of current-stress minimization control. The CSO-UPS control can achieve the minimum current stress i_p in the full power range of p, in these four methods.

B. Efficiency Analysis

In the DAB dc–dc converters, power losses consist of snubber loss, conducting loss in the IGBTs, copper loss in transformer and auxiliary inductors, and core loss in auxiliary inductor. Moreover, ZVS can be achieved at high transmission power, and the dominate portion of the total losses is the conducting loss in IGBT devices [30], which is relative to the average absolute value of inductor current [26], [27], [30]. And conducting loss in IGBT devices can be expressed as

$$P_{\text{cond}} = 4\,|i_L(t)|_{\text{AVG}}\,V_F \tag{17}$$

where V_F is the equivalent forward voltage of IGBT devices and V_F is approximately 1.5 V [3]. $|i_L(t)|_{\text{AVG}}$ represents the average absolute value of inductor current and can be expressed as

$$|i_L(t)|_{\text{AVG}} = \frac{1}{T_s}\int_0^{T_s} |i_L(t)|dt. \tag{18}$$

TABLE III
AVERAGE ABSOLUTE VALUE OF INDUCTOR CURRENT IN FOUR PHASE-SHIFT CONTROL MODES

Phase-shift controls	Range of p	Phase-shift-ratio D_1 (D in SPS)	current $\lvert i_L(t)\rvert_{\mathrm{AVG}}$	
SPS	$0 \le p \le 1$	$\frac{1}{2}-\frac{\sqrt{1-p}}{2}$	$0 \le D \le \frac{k-1}{2k}$	$\frac{4kD^2+k^2-2k+1}{k-1}$
			$\frac{k-1}{2k} \le D \le \frac{1}{2}$	$\frac{8kD-4kD^2+k^2-2k+1}{k+1}$
CSO-DPS	$0 \le p < \frac{k^2+2k-3}{2k^2}$	$1-k\sqrt{\frac{p}{2(k-1)(k+3)}}$ $-1\sqrt{\frac{p}{2(k-1)(k+3)}}$	$\frac{k^3(D_1^2-3D_1+2)+k^2(D_1^2-2D_1+1)}{k^2+k}$ $+\frac{-k(3D_1^2+7D_1-4)+D_1^2-2D_1+1}{k^2+k}$	
	$\frac{k^2+2k-3}{2k^2} < p \le 1$	$\frac{(k-1)}{2}\sqrt{\frac{2(1-p)}{k^2-2k+3}}$	$\frac{k^3-k^3D_1^2+k^2D_1^2-k^2+5kD_1^2-6kD_1}{k^2-k}$ $+\frac{k-D_1^2+2D_1-1}{k^2-k}$	
CSO-EPS	$0 \le p \le \frac{1}{2}$	$\frac{1}{2}+\frac{\sqrt{1-2p}}{2}$	$\frac{k-1}{k} \le D_1 \le 1$	$k^2D_1^2-2D_1+1$ $-k2(D_1^2+2D_1-1)+1$
			$\frac{1}{2} \le D_1 \le \frac{k-1}{k}$	$\frac{k^2-k^2D_1^2+2kD_1^2-2k+1}{k-1}$
	$\frac{1}{2} \le p \le 1$	$\frac{\sqrt{2-2p}}{2}$	$\frac{1}{k} \le D_1 \le \frac{1}{2}$	$-\frac{k^2(D_1^2-1)}{k-1}$ $+\frac{k(2D_1^2-2D_1-1)+1}{k-1}$
			$0 \le D_1 \le \frac{1}{k}$	$\frac{k^2-k^2D_1^2-2kD_1^2}{k+1}$ $+\frac{-2kD_1+k+1}{k+1}$
CSO-UPS	$0 \le p \le 2\frac{k-1}{k^2}$	$1-\frac{\sqrt{2p(k-1)}}{2k-2}$	$2(k+D_1-kD_1-1)(k-kD_1)$	
	$2\frac{k-1}{k^2} \le p \le 1$	$(k-1)\sqrt{\frac{1-p}{k^2-2k+2}}$	$\frac{k^4D_1^2-k^4-k^3D_1^2+k^3-k^2D^2+2k^2D_1}{k^2-k^3+k-1}$ $+\frac{2kD_1^2-2kD_1+k-1}{k^2-k^3+k-1}$	

Combining (9), (10), (18), and Table I, for the convenience of analysis, the unified average absolute value $|i_L(t)|_{\mathrm{AVG}}$ of inductor current with SPS, DPS EPS, and UPS controls can be expressed and unified as Table III.

According to Table III, the relationship curves of the unified average absolute current $|i_L(t)|_{\mathrm{AVG}}$ with respect to the unified transmission power p and voltage conversion ratio k are shown in Fig. 9.

According to Tables II and III and Figs. 8 and 9, the average absolute current $|i_L(t)|_{\mathrm{AVG}}$ can be approximately expressed with current stress i_p and shown as

$$\begin{cases} |i_L(t)|_{\mathrm{AVG}} = \dfrac{1}{2}(k-kD_1)i_p & \left(0 \le p \le 2\dfrac{k-1}{k^2}\right) \\ |i_L(t)|_{\mathrm{AVG}} \approx \dfrac{1}{2}i_p & \left(2\dfrac{k-1}{k^2} < p \le 1\right). \end{cases} \tag{19}$$

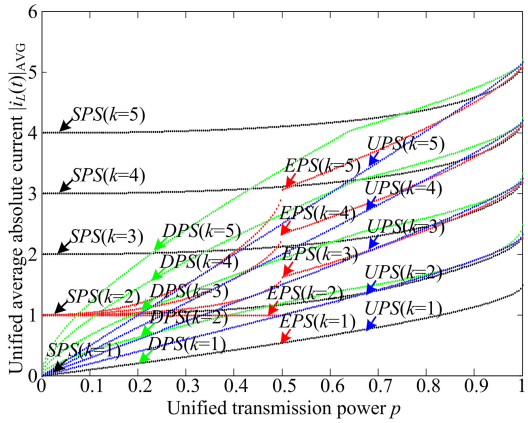

Fig. 9. Relation curves of i_{av} with respect to p and k in SPS, CSO-DPS, CSO-EPS, and CSO-UPS controls.

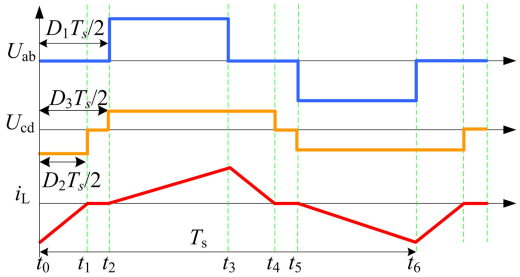

Fig. 10. Waveforms of U_{ab}, U_{cd}, and i_L in the CSO-UPS control at the light load.

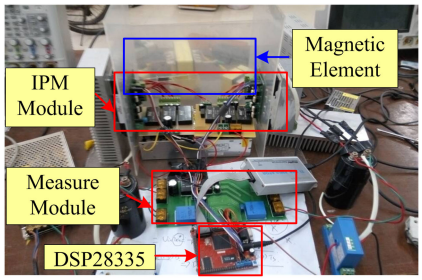

Fig. 11. Experimental hardware prototype.

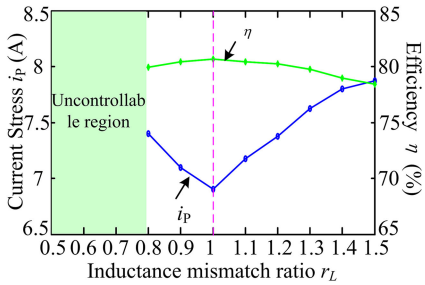

Fig. 12. Experimental curve of the current stress and efficiency with respect to r_L in the traditional CSO-DPS control.

According to (19), if the voltage ratio k is much higher than 1, the waveform shape of current i_L is similar to a triangle in high transmission power p condition. And the shape of the current waveform i_L is equivalent to a triangle at the light load. In this triangle, the current stress i_p is equivalent to the height of the triangle. And the average absolute current $|i_L(t)|_{\mathrm{AVG}}$ is proportional to the area of the triangle. The unified current stress is double of the unified average absolute current. Thus, $|i_L(t)|_{\mathrm{AVG}}$ can be reduced and associated with the decrease of current stress, which brings the conducting loss reduction in the IGBTs, finally. And the converter can gain a high efficiency at the high transmission power.

Moreover, the snubber loss occupies the major portion of the total losses at the light load without the pure ZVS operation of the converter [30]. Although the ZVS operation is not the key point in this paper, the high efficiency may be also obtained by using the CSO-UPS control. According to (9), the waveforms of U_{ab}, U_{cd}, and i_L in CSO-UPS control at the light load can be further described as Fig. 10.

Combining Figs. 3 and 10, it is clear that switches S_3, S_4, S_5, S_6, S_7, and S_8 can be realized with zero-current switching (ZCS), and switches S_1 and S_2 are switched at the peak current

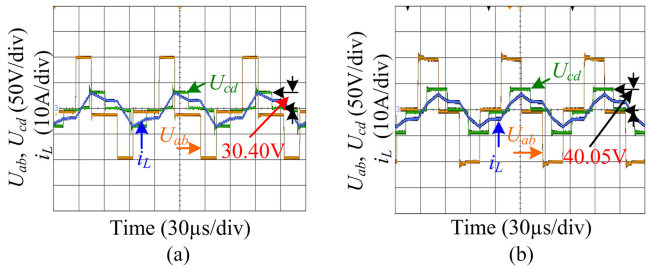

Fig. 13. Experimental waveforms of U_{ab}, U_{cd}, and i_L with $r_L = 0.6$. (a) Traditional CSO-DPS control. (b) Simple CSO-DPS control.

to guarantee quasi-ZVS. Thus, the converter can also gain high efficiency at the light load, too.

V. Experimental Analysis

In order to verify the aforementioned theoretical analysis, a scale-down laboratory prototype is designed, and the main parameters of the DAB dc–dc converter are as follows: transformer's turns ratio $n = 1$, auxiliary inductor $L_r = 0.2$ mH, transformer leakage inductor is close to zero, and the switching frequency $f_s = 10$ kHz. The photo of the laboratory prototype is shown in Fig. 11.

A. Inductor Sensitivity Analysis of Traditional CSO Scheme

Due to the requirement of inductor parameter to realize the traditional CSO-DPS scheme [23], the inductor parameter mismatch may result an impact on the performance of current stress reduction.

Here, the ratio r_L of the adopted inductor parameter L_n in the traditional CSO-DPS controller to the actual value is defined as

$$r_L = \frac{L_n}{L}. \tag{20}$$

It is defined that $U_{\mathrm{in}} = 100$ V, $R = 20\ \Omega$, and the desired output voltage $U_o^* = 40$ V; Fig. 12 shows experimental curves of current stress and efficiency with respect to r_L in traditional CSO-DPS control. In this figure, the minimum current stress i_p can reach at $r_L = 1$ (no inductance mismatch). In Fig. 12, the current stress i_p increases as r_L is far away from 1, and the efficiency η decreases as r_L is far away from 1. In addition, when r_L is approximately less than 0.7, the converter falls into an uncontrollable region, where the large value of D_1 is estimated with the small unified power transmission p, and the phase-shift ratio D_2 reaches the upper limit as $(1 - D_1)$ in the case of $D_2 \le D_1$. In this region, the output voltage U_o can never reach the desired output voltage U_o^*, as shown in Fig. 13.

From Figs. 12 and 13, it is clear that inductor parameter mismatch will result an impact on the performance of the traditional CSO-DPS scheme and that the converter may fall into an uncontrollable region with smaller r_L. Fortunately, the simple CSO-DPS scheme can overcome this drawback of the traditional method.

B. Experimental Comparison of Current Stress and Efficiency

When the output voltage is set to $U_o = 40$ V, Fig. 14 shows experimental curves of current stress with respect to voltage

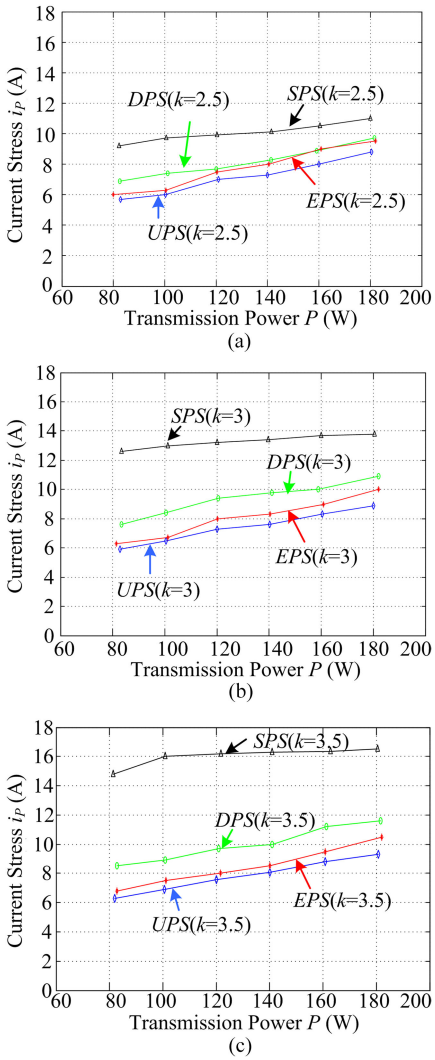

Fig. 14. Experimental curves of current stress with respect to P in four control methods in various voltage conversion ratio k conditions. (a) $k = 2.5$, (b) $k = 3$, and (c) $k = 3.5$.

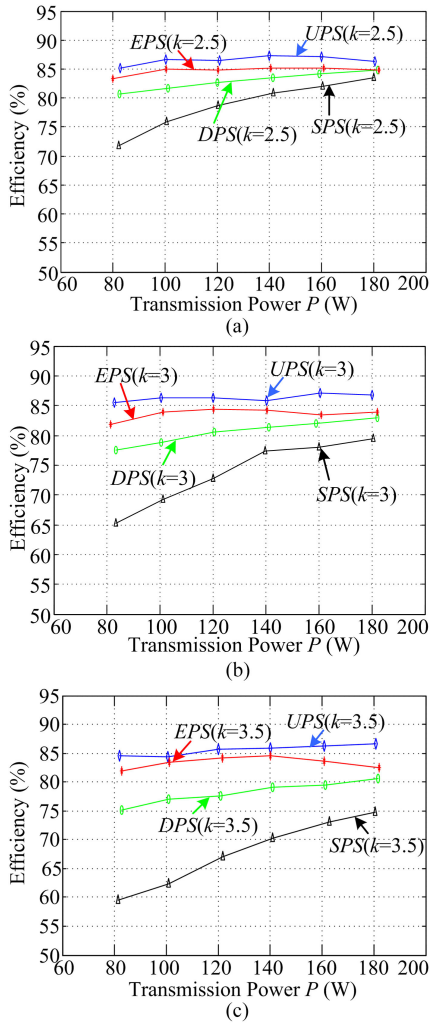

Fig. 15. Curves of the efficiency varied with P in four control methods in various voltage conversion ratio k conditions. (a) $k = 2.5$, (b) $k = 3$, and (c) $k = 3.5$.

conversion ratio k and transmission power P in these four control schemes. From Fig. 14, if the transmission power P is invariable, the current stress i_p in these four control methods increase with k. And if k is invariable, the current stress i_p in these four control methods increases with P, too. In addition, both CSO-DPS control and CSO-UPS control can gain lower current stress than SPS control. And the CSO-UPS control can realize the lowest current stress in the four control methods.

In the same experimental conditions with Fig. 14, Fig 15 shows the efficiency curves of the adopted converter with respect to k and P in these four control methods. According to Fig. 15, both of CSO-DPS and CSO-UPS controls can obtain higher efficiency than SPS control. And the CSO-UPS control can achieve the highest efficiency in the four control methods.

From Figs. 14 and 15, the experimental results indicate that to reduce current stress is an alternative solution to improve the efficiency of DAB dc–dc converters, and the proposed CSO-UPS control can gain the lowest current stress and the highest efficiency in the four phase-shift controls.

VI. Conclusion

A simple current-stress-optimized scheme with UPS control has been proposed in this paper. The relationships of the proposed CSO-UPS, CSO-DPS, CSO-EPS, and SPS control schemes are discussed and compared in detail. An experimental scale-down prototype test is adopted to investigate the performance of the traditional CSO-DPS scheme and to compare the performance of these four phase-shift control schemes. The conducted studies are summarized as follows:

1) In the traditional CSO scheme, the inductor parameter mismatch will result an impact on current stress reduction and the converter may fall into an uncontrollable region. But the proposed simple CSO scheme is not sensitive to inductance mismatch.
2) Compared with traditional CSO method, the proposed simple CSO scheme can be realized without inductor parameters and the load-current value. And the computation complexity of the simple CSO scheme can be significantly reduced.
3) The UPS control mode can be simplified as the conventional DPS, SPS, and EPS modes in the special conditions

such as SPS ($D_1 = 0$ and $D_2 = D_3$), DPS ($D_1 = D_3 - D_2$), EPS ($D_3 - D_2 = 0$ or $D_1 = 0$).

4) The simple CSO-UPS control can obtain the lowest current stress and the highest efficiency in these four kinds of phase-shift control modes.

REFERENCES

[1] R. W. A. A. De Doncker, D. M. Divan, and M. H. Kheraluwala, "A three-phase soft-switched high-power-density DC/DC converter for high-power applications," *IEEE Trans. Ind. Appl.*, vol. 27, no. 1, pp. 63–73, Aug. 1991.

[2] D. Aggeler, J. Biela, S. Inoue, H. Akagi, and J. W. Kolar, "Bi-directional isolated dc–dc converter for next-generation power distribution-comparison of converters using Si and SiC devices," in *Proc. Power Convers. Conf.*, Nagoya, Japan, Apr. 2007, pp. 510–517.

[3] X. Li and Y. Li, "An optimized phase-shift modulation for fast transient response in a dual-active-bridge converter," *IEEE Trans. Power Electron.*, vol. 29, no. 6, pp. 2661–2665, Jan. 2014.

[4] H. J. Chiu and L. W. Lin, "A bidirectional DC–DC converter for fuel cell electric vehicle driving system," *IEEE Trans. Power Electron.*, vol. 21, no. 4, pp. 950–958, Jul. 2006.

[5] N. M. L. Tan, T. Abe, and H. Akagi, "Design and performance of a bidirectional isolated DC–DC converter for a battery energy storage system," *IEEE Trans. Power Electron.*, vol. 27, no. 3, pp. 1237–1248, Mar. 2012.

[6] C. Mi, H. Bai, C. Wang, and S. Gargies, "Operation, design and control of dual H-bridge-based isolated bidirectional DC–DC converter," *IET Power Electron.*, vol. 1, no. 4, pp. 507–517, Dec. 2008.

[7] H. Bai, C. C. Mi, and S. Gargies, "The short-time-scale transient processes in high-voltage and high-power isolated bidirectional DC–DC converters," *IEEE Trans. Power Electron.*, vol. 23, no. 6, pp. 2648–2656, Nov. 2008.

[8] H. Akagi and R. Kitada, "Control and design of a modular multilevel cascade BTB system using bidirectional isolated DC/DC converters," *IEEE Trans. Power Electron.*, vol. 26, no. 9, pp. 2457–2464, Sep. 2011.

[9] C. Zhao, S. D. Round, and J. W. Kolar, "An isolated three-port bidirectional DC–DC converter with decoupled power flow management," *IEEE Trans. Power Electron.*, vol. 23, no. 5, pp. 2443–2453, Sep. 2008.

[10] F. Krismer and J. W. Kolar, "Accurate small-signal model for the digital control of an automotive bidirectional dual active bridge," *IEEE Trans. Power Electron.*, vol. 24, no. 12, pp. 2756–2768, Dec. 2009.

[11] F. Krismer and J. W. Kolar, "Accurate power loss model derivation of a high-current dual active bridge converter for an automotive application," *IEEE Trans. Ind. Electron.*, vol. 57, no. 3, pp. 881–891, Mar. 2010.

[12] G. Oggier, M. Ordonez, M. Galvez, and F. Luchino, "Fast transient boundary control and steady-state operation of the dual active bridge converter using the natural switching surface," *IEEE Trans. Power Electron.*, vol. 29, no. 2, pp. 946–957, Feb. 2014.

[13] D. Segaran, D. G. Holmes, and B. P. McGrath, "Enhanced load step response for a bidirectional dc–dc converter," *IEEE Trans. Power Electron.*, vol. 28, no. 1, pp. 371–379, Jan. 2013.

[14] J. Hiltunen, V. Väisänen, R. Juntunen, and P. Silventoinen, "Variable-frequency phase shift modulation of a dual active bridge converter," *IEEE Trans. Power Electron.*, vol. 30, no. 12, pp. 7138–7148, Dec. 2015.

[15] F. Krismer and J. W. Kolar, "Efficiency-optimized high-current dual active bridge converter for automotive applications," *IEEE Trans. Ind. Electron.*, vol. 59, no. 7, pp. 2745–2760, Jul. 2012.

[16] S. Inoue and H. Akagi, "A bi-directional isolated DC/DC converter as a core circuit of the next-generation medium-voltage power conversion system," in *Proc. 37th Power Electron. Spec. Conf.*, Jeju, Korea, Jun. 2006, pp. 1–7.

[17] A. K. Jain and R. Ayyanar, "PWM control of dual active bridge: Comprehensive analysis and experimental verification," *IEEE Trans. Power Electron.*, vol. 26, no. 4, pp. 1215–1227, Apr. 2011.

[18] H. Bai and C. Mi, "Eliminate reactive power and increase system efficiency of isolated bidirectional dual-active-bridge DC–DC converters using novel dual-phase-shift control," *IEEE Trans. Power Electron.*, vol. 23, no. 6, pp. 2905–2914, Sep. 2008.

[19] H. Bai, Z. Nie, and C. Mi, "Experimental comparison of traditional phase-shift, dual-phase-shift, and model-based control of isolated bidirectional DC–DC converters," *IEEE Trans. Power Electron.*, vol. 25, no. 6, pp. 1444–1449, Jun. 2010.

[20] B. Zhao, Q. Song, and W. Liu, "Power characterization of isolated bidirectional dual-active-bridge DC–DC converter with dual-phase-shift control," *IEEE Trans. Power Electron.*, vol. 27, no. 9, pp. 4172–4176, Sep. 2012.

[21] M. Kim, M. Rosekeit, S. K. Sul, and R. De Doncker, "A dual-phase-shift control strategy for dual-active-bridge DC–DC converter in wide voltage range," in *Proc. 8th Int. Conf. Power Electron. ECCE Asia*, Jeju, Korea, Jun. 2011, pp. 364–371.

[22] B. Zhao, Q. Yu, and W. Sun, "Extended-phase-shift control of isolated bidirectional DC–DC converter for power distribution in microgrid," *IEEE Trans. Power Electron.*, vol. 27, no. 11, pp. 4667–4680, Nov. 2012.

[23] B. Zhao, Q. Song, W. Liu, and W. Sun, "Current-stress-optimized switching strategy of isolated bidirectional DC–DC converter with dual-phase-shift control," *IEEE Trans. Ind. Electron.*, vol. 60, no. 10, pp. 4458–4467, Oct. 2013.

[24] A. Rodríguez, A. Vázquez, D. G. Lamar, M. M. Hernando, and J. Sebastian, "different purpose design strategies and techniques to improve the performance of a dual active bridge with phase-shift control," *IEEE Trans. Ind. Electron.*, vol. 30, no. 2, pp. 790–804, Feb. 2015.

[25] G. G. Oggier, G. O. García, and A. R. Oliva, "Modulation strategy to operate the dual active bridge DC–DC converter under soft switching in the whole operating range," *IEEE Trans. Ind. Electron.*, vol. 26, no. 4, pp. 1228–1236, Apr. 2011.

[26] G. Oggier and R. Oliva, "Switching control strategy to minimize dual active bridge converter losses," *IEEE Trans. Power Electron.*, vol. 24, no. 7, pp. 1826–1838, Jul. 2009.

[27] B. Zhao, Q. Yu, and W. Sun, "Efficiency characterization and optimization of isolated bidirectional DC–DC converter based on dual-phase-shift control for DC distribution application," *IEEE Trans. Ind. Electron.*, vol. 28, no. 4, pp. 1171–1727, Jul. 2013.

[28] F. Krismer and J. W. Kolar, "Closed form solution for minimum conduction loss modulation of DAB converters," *IEEE Trans. Power Electron.*, vol. 27, no. 1, pp. 174–188, Jan. 2012.

[29] Y. Shi, R. Li, Y. Xue, and H. Li, "Optimized operation of current-fed dual active bridge DC–DC converter for PV Applications," *IEEE Trans. Ind. Electron.*, vol. 62, no. 11, pp. 6986–6995, Nov. 2015.

[30] S. Inoue and H. Akagi, "A bidirectional DC–DC converter for an energy storage system with galvanic isolation," *IEEE Trans. Power Electron.*, vol. 22, no. 6, pp. 2299–2306, Nov. 2007.

[31] B. Zhao, Q. Song, W. Liu, and Y. Sun, "Overview of dual-active-bridge isolated bidirectional DC–DC converter for high-frequency-link power-conversion system," *IEEE Trans. Power Electron.*, vol. 29, no. 8, pp. 4091–4106, Aug. 2014.

Nie Hou was born in Mianyang, Sichuan, China, in 1990. He received the B.S. degree in electrical engineering from Southwest Jiaotong University, Chengdu, China, in 2014, where he is currently working toward the M.S degree in electrical engineering.

His current research interests include digital control and optimization methods of DC–DC converter and DC distribution system.

Wensheng Song (M'13) received the B.S. degree in electronic and information engineering and the Ph.D. degree in electrical engineering from Southwest Jiaotong University, Chengdu, China, in 2006 and 2011, respectively.

He is currently a Lecturer in the school of Electrical Engineering, Southwest Jiaotong University. From Sep. 2009 to Sep. 2010, he was a Visiting Scholar with the Department of Electrical Engineering and Computer Science, University of California, Irvine, USA. From Jul. 2015 to Dec. 2015, he is a Visiting Scholar at the University of Alberta, Edmonton, Canada. His current research interests include digital control and modulation methods of electrical AC–DC–AC railway traction drive systems, and multilevel converters.

Mingyi Wu was born in Xiangyang, Hubei, China, in 1992. He received the B.S. degree in electrical engineering from Southwest Jiaotong University, Chengdu, China, in 2015, where he is currently working toward the M.S degree in electrical engineering.

His current research interests include power electronics and motor drives.